Commun. Comput. Phys.
doi: 10.4208/cicp.250913.080414a

Vol. **16**, No. 4, pp. 1081-1101
October 2014

Simulation of Propagating Acoustic Wavefronts with Random Sound Speed

Sheri L. Martinelli*

Undersea Warfare Weapons, Vehicles, and Defensive Systems Department, Naval Undersea Warfare Center, Newport, Rhode Island 02841, USA.

Received 25 September 2013; Accepted (in revised version) 8 April 2014

Available online 12 August 2014

Abstract. A method for simulating acoustic wavefronts propagating under random sound speed conditions is presented. The approach applies a level set method to solve the Eikonal equation of high frequency acoustics for surfaces of constant phase, instead of tracing rays. The Lagrangian nature often makes full-field ray solutions difficult to reconstruct. The level set method captures multiple-valued solutions on a fixed grid. It is straightforward to represent other sources of uncertainty in the input data using this model, which has an advantage over Monte Carlo approaches in that it yields an expression for the solution as a function of random variables.

AMS subject classifications: 60H35, 65M70, 65C20

Key words: Level set method, wavefront methods, high-frequency acoustic propagation, stochastic collocation.

1 Introduction

Modeling and simulation of underwater sound propagation in shallow water environments is critical to the design of acoustic systems and system performance evaluation. Although not a full substitute for in-water operational testing, access to high fidelity simulation can drastically reduce the need for expensive, risky, in-water experiments. One such family of applications involves high frequency active arrays operating in environments where reverberation dominates the noise field. Transmit frequencies at least on the order of 10 kHz render full wave equation simulations computationally impractical due to the need for high mesh resolution in space and time.

*Corresponding author. *Email address:* sheri_martinelli@alumni.brown.edu (S. L. Martinelli)

For this reason, it is common to apply the geometric acoustics (geometric optics) approximation, c.f. Chapter 3 in [1], to the linear wave equation for the acoustic pressure,

$$p_{tt} - c(\mathbf{x})^2 \triangle p = 0, \tag{1.1}$$

$$p(t,\mathbf{x}) \approx e^{i\omega S(t,\mathbf{x})} \sum_{k=0}^{\infty} A_k(t,\mathbf{x})(i\omega)^{-k}, \tag{1.2}$$

to yield an Eikonal equation for the acoustic phase:

$$S(t,\mathbf{x}) \pm c|\nabla S(t,\mathbf{x})| = 0, \tag{1.3}$$

and a transport equation for the first amplitude term:

$$(A_0)_t + c(\mathbf{x}) \frac{\nabla S \cdot \nabla A_0}{|\nabla S|} + \frac{c(\mathbf{x})^2 \triangle S - S_{tt}}{2c(\mathbf{x})|\nabla S|} A_0 = 0. \tag{1.4}$$

Eq. (1.2) is based on a WKB expansion about the large parameter ω. The standard computational approach to solving the nonlinear equation (1.3) is ray tracing, which is based on the method of characteristics. This is a Lagrangian method: the user specifies initial conditions for a number of rays, i.e., location and starting angles from an initial wavefront, and solves for the resulting trajectories defined by the system with Hamiltonian $H(\mathbf{x},\mathbf{k}) = c(\mathbf{x})|\mathbf{k}|$, where $\mathbf{k}$ is the generalized momentum vector. Examples of applications that rely on ray tracing for system design and performance prediction include acoustic tomography [2] and underwater communications [3]. In acoustic tomography, accurate travel time data between a source and receiver over long ranges are used to infer information about ocean currents and temperatures. Both applications have a need for sorting out multi-path time arrivals that occur as a result of ray bending, and surface and bottom scattering. The ray approach has many known limitations. In particular, the Lagrangian nature of the model leads to difficulty resolving wave arrivals at a fixed location in space since the user does not have control over the spatial discretization beyond the source. That is, small perturbations in the ray shooting angle can lead to significantly differing trajectories. This is especially true in range-dependent, shallow water environments where reflections from rough surfaces may scatter the trajectories further. Hence there is benefit to consider fixed frame of reference approaches. Toward that end, [4] proposes applying the level set method [5,6] to the problem of high frequency underwater acoustic propagation. The level sets approach solves the Eikonal equation (1.3) in the phase space $(\mathbf{x},\mathbf{k})$ by representing the initial wavefront as the zero level set of a vector-valued function $\mathbf{\Phi}(t,\mathbf{x},\mathbf{k})$ in the higher-dimensional space. The wavefronts propagate according to the velocity field determined by the local ray direction, but on a fixed spatial grid. One recovers the wavefront at time t by projecting the zero level set of $\mathbf{\Phi}(t,\mathbf{x},\mathbf{k})$ back into the physical space.

The intent of this work is to extend the method outlined in [4] to generate realizations of propagating wavefronts in the presence of random perturbations in the sound

speed profile. In fact, existing simulations tend to treat the acoustic environment in a deterministic manner, incorporating the uncertainty in post-processing. For example, a point scattering approach to simulating reverberation takes the results of a deterministic ray trace and adds randomness to the arrival times and arrival angles of the rays at the receiver. The assumption these models make is that the variation in arrival time and angle of a ray at the receiver due to unknown or un-modeled environment aspects is small. However, even small perturbations can have a drastic effect on the resulting ray trajectories. It has been shown [7] that under weak sound speed fluctuations, wavefronts exhibit greater stability than rays, in the sense that the significant ray perturbations tend to occur *along* the wavefronts rather than *across* them. Thus a wavefront propagation algorithm that incorporates uncertainty in the environmental parameters is potentially a very useful tool for design and testing of acoustic systems. The present work seeks to incorporate the uncertainty directly into the environment model and use this information to construct solutions on a fixed grid. So two difficulties are addressed: first, the method solves the relevant equations on a fixed grid to eliminate the need to interpolate over increasingly sparse ray arrivals, and second, the model includes the uncertainty where it occurs (the environment). Thus this type of approach offers improved simulation fidelity.

1.1 Related work

The work presented here is based on the foundation and results proposed in [4] and [8]. Those efforts explored the application of a level set method described in [6] to problems in underwater acoustic propagation.

The approach to managing environmental uncertainty is based on the work of Xiu and Hesthaven [9], which presents a stochastic collocation approach to solving partial differential equations involving non-white processes. Stochastic collocation is built on the framework of polynomial chaos expansions in terms of random variables. If the uncertainty is in the form of a stochastic process, one first applies a Karhunen-Loève expansion to obtain an expression of the process in terms of independent (or uncorrelated as it may be) random variables. Classical stochastic calculus approaches assume idealized, white (uncorrelated) processes, whereas most physical processes do have some manner of correlation that cannot be neglected. Monte Carlo techniques — the standard for these types of problems — are effective and easy to implement, but suffer from slow convergence. Stochastic collocation methods using deterministic sampling approaches converge very fast for certain processes, though the performance depends on the dimension of the random space. Chauviere, Hesthaven and Lurati later applied the method to computational electromagnetics in [10]. Nobile, Tempone and Webster undertook a study of stochastic collocation on sparse grids for elliptic and diffusion equations [11]. The works of Preston, et al. [12], and later that of Pätz and Preusser [13] apply similar techniques to related problems in biomedical engineering and image segmentation, respectively. However their applications differ from the present work in the underlying physics and the use of level set functions.

1.2 Outline

In [4], a method is described for computing solutions to the deterministic transport (or level set) equation,

$$f_t + c(x,z)\cos(\theta) f_x + c(x,z)\sin(\theta) f_z + (c_x \sin(\theta) - c_z \cos(\theta)) f_\theta = 0, \tag{1.5}$$

alternately,

$$\begin{aligned} &\frac{\partial f}{\partial t} = \mathcal{L} f, \\ &\mathcal{L} = -\mathbf{V} \cdot \nabla, \end{aligned} \tag{1.6}$$

representing two-dimensional propagation in a water column with symmetry in the y-direction, e.g. an infinite line source. Eq. (1.5) is a Liouville equation that evolves an initial wavefront in the direction of its normal vector which is the local ray direction, where $c(x,z)$ is the wave speed in the medium. The Liouville equation is solved for a vector level set function $\mathbf{\Phi}(t,x,z,\theta)$ with two components. The wavefront at a fixed time t may be extracted as the intersection of the zero level sets of the two components.

This work addresses the case of a wave speed given by $c(x,z;\vec{\xi})$, with $(x,z) \in D \subset \mathbb{R}^2$, and a random vector $\vec{\xi}$ taking values in a probability space $(\Omega,\mathcal{F},\mathcal{P})$. In the usual notation, Ω is the sample space, $\mathcal{F}$ is the σ-algebra of events in Ω, and $\mathcal{P}$ is the probability measure on the space. Assume that $c(x,z;\vec{\xi})$ has the form

$$c(x,z;\vec{\xi}) = c_0(x,z) + \epsilon c'(x,z;\vec{\xi}), \tag{1.7}$$

with $c'(x,z;\vec{\xi})$ a zero-mean process, and ϵ is a small, non-negative constant used here to illustrate that the uncertainty is a result of small perturbations to the sound speed.

Section 2 provides background on the tools applied in the proposed model. Section 3 derives the relevant expansions for a single parameter expansion where $c'(x,z;\xi)$ is a uniform random variable, then extends it to allow $c'(x,z;\vec{\xi})$ to be a zero-mean Gaussian random field on the physical space. The Gaussian assumption is not a limitation, but offers mathematical convenience. Finally we present some numerical examples in Section 4 and conclude in Section 5. Although the work presented here limits its scope to a single random input parameter, the sound speed, the approach is general and directly applicable to other sources of uncertainty.

2 Background

2.1 The level set method

The level set method is derived from the Hamilton-Jacobi form of (1.3),

$$S_t(t,\mathbf{x}) + H(\mathbf{x},\mathbf{k}) = 0, \tag{2.1}$$

$$H(\mathbf{x},\mathbf{k}) = c(\mathbf{x})|\mathbf{k}|. \tag{2.2}$$

The momentum $\mathbf{k}$ is identified with ∇S. The Hamiltonian is conservative, i.e., $H(\mathbf{x},\mathbf{k})$ satisfies $\frac{\partial H}{\partial t}=0$, thus H is constant so that (taking $H\equiv 1$) $|\mathbf{k}|=\frac{1}{c}$. This allows one to reduce the dimension of full phase space by one. If $\mathbf{x}\in\mathbb{R}^2$ for instance, then $\mathbf{k}=(\frac{\cos\theta}{c},\frac{\sin\theta}{c})$ and one need only consider θ as an independent variable in phase space. The bicharacteristic strips, $(\mathbf{x},\mathbf{k})$, satisfy the relations

$$\dot{\mathbf{x}}(t)=\nabla_k H(\mathbf{x},\mathbf{k})=c(\mathbf{x}(t))\frac{\mathbf{k}(t)}{|\mathbf{k}(t)|}, \tag{2.3a}$$

$$\dot{\mathbf{k}}(t)=-\nabla_x H(\mathbf{x},\mathbf{k})=-|\mathbf{k}(t)|\nabla_x c(\mathbf{x}(t)). \tag{2.3b}$$

Restricting to propagation in two-dimensional physical space with $\mathbf{x}=(x_1,x_2)$, Eqs. (2.3) reduce to

$$\dot{x_1}(t)=c(x_1(t),x_2(t))\cos\theta(t), \tag{2.4a}$$

$$\dot{x_2}(t)=c(x_1(t),x_2(t))\sin\theta(t), \tag{2.4b}$$

$$\dot{\theta}(t)=\frac{\partial c}{\partial x_1}\sin\theta(t)-\frac{\partial c}{\partial x_2}\cos\theta(t). \tag{2.4c}$$

Consider the zero level set of a function $\mathbf{\Phi}(t,x_1(t),x_2(t),\theta(t))=0$. Differentiating with respect to time shows that $\mathbf{\Phi}$ satisfies a Liouville equation (c.f. Eq. (1.5))

$$\mathbf{\Phi}_t+\mathbf{V}\cdot\nabla\mathbf{\Phi}=0 \tag{2.5}$$

with

$$\mathbf{V}=\begin{pmatrix}\dot{x_1}(t)\\ \dot{x_2}(t)\\ \dot{\theta}(t)\end{pmatrix}. \tag{2.6}$$

This is the premise of the level set method. By embedding the initial wavefront in the zero level set of a function defined in the reduced phase space, one may propagate the surface using the first-order transport equation (2.5). The velocity field $\mathbf{V}$ is defined by the ray equations (2.4).

2.2 Generalized polynomial chaos

The generalized Polynomial Chaos (gPC) expansion is a function expansion in terms of an orthogonal polynomial basis on the probability space $(\Omega,\mathcal{F},\mathcal{P})$ as follows. Let ξ be a random variable, $\xi:\Omega\to\mathbb{R}$ with distribution function $F(y)=P(\xi\leq y)$ and finite moments $\mathbb{E}\left[|\xi|^{2m}\right]=\int|y|^{2m}\mathrm{d}F(y)<\infty, m=0,\cdots,N_p$. The gPC expansion of a univariate function $f(s;\xi)$ dependent on the random variable ξ is then

$$f_{\mathrm{gPC}}(s;\xi)=\sum_{n=0}^{N_p}\hat{f}_n(s)\psi_n(\xi). \tag{2.7}$$

The orthogonality condition for the gPC basis functions is

$$\mathbb{E}[\psi_n(\xi)\psi_m(\xi)] = \int \psi_n(\xi)\psi_m(\xi)w(\xi)\,\mathrm{d}\xi = \gamma_n\delta_{nm}, \tag{2.8}$$

where δ_{nm} is the Kronecker delta, $w(\xi)$ is a weight function with respect to which the basis functions are orthogonal, and $\gamma_n = \mathbb{E}[\psi_n^2(\xi)]$. Thus, a good choice of basis functions are those satisfying (2.8) with respect to a weight function that corresponds to the distribution $F(\xi)$. That is, the weight function $w(\xi)$ is related in form to the probability density function (PDF) $\rho(\xi)$ defined as $\mathrm{d}F(\xi) = \rho(\xi)\mathrm{d}\xi$. The orthogonality condition leads to the expression for the coefficients $\hat{f}_n(s)$:

$$\hat{f}_n(s) = \frac{1}{\gamma_n}\int f(s;\xi)\psi_n(\xi)\rho(\xi)\,\mathrm{d}\xi. \tag{2.9}$$

2.2.1 Expansion in a uniform random variable

Let $\xi \sim U[-1,1]$ be a uniformly distributed random variable on the interval $[-1,1]$, with PDF

$$\rho(\xi) = \begin{cases} \frac{1}{2}, & -1 \le \xi \le 1, \\ 0, & \text{otherwise.} \end{cases} \tag{2.10}$$

One can always transform ξ to a $U[a,b]$ random variable by $\tilde{\xi} = \left(\frac{b-a}{2}\right)\xi + \frac{b+a}{2}$. The requirement (2.8) then implies that an expansion in Legendre polynomials is appropriate, with normalization constant $\tilde{\gamma}_n = \frac{1}{2n+1}$ which is scaled by a factor of $\frac{1}{2}$ to account for the PDF scaling.

2.2.2 Expansion in a Gaussian random variable

Let $\xi \sim N(0,1)$ be a standard Gaussian random variable (i.e., zero-mean and variance $\sigma^2 = 1$), defined on $\mathbb{R}$, with PDF

$$\rho(\xi) = \frac{1}{\sqrt{2\pi}}e^{-\xi^2/2}. \tag{2.11}$$

One can always transform ξ to a $N(\mu,\sigma^2)$ random variable by $\tilde{\xi} = \sigma\xi + \mu$. The orthogonality condition (2.8) then implies that an expansion in Hermite polynomials is appropriate, with normalization constant $\gamma_n = n!$. As in [14], the definition of Hermite polynomials applied here is modified from the classical Hermite polynomials to account for the scaling in the PDF. The modified Hermite polynomials satisfy the three-term recursion

$$H_0(\xi) = 1, \tag{2.12a}$$
$$H_1(\xi) = \xi, \tag{2.12b}$$
$$H_{n+1}(\xi) = \xi H_n(\xi) - nH_{n-1}(\xi), \quad n = 1,2,\cdots. \tag{2.12c}$$

2.2.3 Multivariate expansion

It is rarely the case that there is only one source of uncertainty in a system. Also many sources of uncertainty are more realistically modeled as a random process and require characterization in several random variables (c.f. Section 2.3).

Consider now a d-dimensional random vector with mutually independent components $\vec{\xi}=(\xi_1,\cdots,\xi_d)$. Independence ensures that the distribution $F_{\vec{\xi}}(\xi_1,\cdots,\xi_d)=\prod_{i=1}^{d}F_{\xi_i}(\xi_i)$, where $F_{\xi_i}(\xi_i)$ is the marginal distribution of ξ_i. Let each ξ_i be associated with a gPC basis $\{\psi_k(\xi_i)\}_{k=0}^{N_p}$ for $\mathbb{P}_{N_p}(\xi_i)$, the space of polynomials of degree at most N_p in ξ_i. Define a multi-index $\mathbf{i}=(i_1,\cdots,i_d)$ and let $|\mathbf{i}|=i_1+\cdots+i_d$. Then a gPC basis for $\mathbb{P}_{N_p}^d$, the space of d-variate polynomials of degree at most N_p, may be defined as $\left\{\mathbf{\Psi}(\vec{\xi})\right\}_{|\mathbf{i}|=0}^{N_p}$ where

$$\mathbf{\Psi}_{\mathbf{i}}(\vec{\xi})=\psi_{i_1}(\xi_1)\psi_{i_2}(\xi_2)\cdots\psi_{i_d}(\xi_d). \tag{2.13}$$

Again owing to the independence assumption, the orthogonality relation is

$$\mathbb{E}\left[\mathbf{\Psi}_{\mathbf{i}}(\vec{\xi})\mathbf{\Psi}_{\mathbf{j}}(\vec{\xi})\right]=\gamma_{\mathbf{i}}\delta_{\mathbf{ij}}, \tag{2.14}$$

where $\gamma_{\mathbf{i}}=\gamma_{i_1}\cdots\gamma_{i_d}$ and $\delta_{\mathbf{ij}}=\delta_{i_1j_1}\cdots\delta_{i_dj_d}$. The space $\mathbb{P}_{N_p}^d$ has dimension $\binom{N_p+d}{N_p}$ [14]. The generalization of (2.7) is then

$$f_{\mathrm{gPC}}(s;\vec{\xi})=\sum_{|\mathbf{n}|=0}^{N_p}\hat{f}_{\mathbf{n}}(s)\mathbf{\Psi}_{\mathbf{n}}(\vec{\xi}). \tag{2.15}$$

2.3 Karhunen-Loève expansion

To apply the techniques discussed in this work, it is necessary to express the uncertainty in terms of a finite number of mutually independent random variables. Let $X(s)\equiv X(s;\omega),\omega\in\Omega$, be a random process on $[0,S]\times\Omega$ with covariance $K_x(r,s)$. Without loss of generality, assume that $X(s)$ is a zero-mean process to simplify notation.

The Karhunen-Loève (KL) expansion provides a partial characterization of the process in terms of a series expansion in orthogonal functions,

$$X(s,\omega)=m_X(s)+\sum_{i=1}^{\infty}\varphi_i(s)X_i(\omega),\quad 0\le s\le S. \tag{2.16}$$

This provides only a partial characterization in the sense that it is a second moment characterization; it is a full characterization for Gaussian processes however. The orthogonality corresponds to the condition that the X_i are uncorrelated, i.e.,

$$\mathbb{E}\left[X_iX_j\right]=\lambda_i\delta_{ij}. \tag{2.17}$$

The λ_i correspond to the expected energy of the component $\varphi_i(s)$. The random variables are defined by

$$X_i = \int_0^S X(s,\omega)\varphi_i(s)\,\mathrm{d}s. \tag{2.18}$$

The λ_i and $\varphi_i(s)$ are eigenvalue - eigenfunction pairs that solve the integral equation [15]

$$\lambda_i\varphi_i(s) = \int_0^S K_x(r,s)\varphi_i(r)\,\mathrm{d}r. \tag{2.19}$$

It is worth noting that this expansion requires that the values of s be restricted to a compact set.

We restrict our consideration to Gaussian processes for the following reasons:

1. The central limit theorem suggests that the Gaussian model is appropriate for many physical systems [14].

2. The X_i in (2.18) are Gaussian by definition, if $X(s,\omega)$ is a Gaussian process.

3. Since the X_i are Gaussian and uncorrelated by design, they are independent; so the multivariate gPC assumptions are satisfied.

In light of (2.17), one may express (2.16) in terms of standard $N(0,1)$ random variables,

$$X(s,\omega) = \sum_{i=1}^{\infty} \sqrt{\lambda_i}\varphi_i(s)\xi_i(\omega), \quad 0 \le s \le S. \tag{2.20}$$

It is not always the case that the Gaussian model is an appropriate one. For instance, it may not always be realistic to model certain phenomena such as scattering to take values over the real line. Even allowing the sound speed profile to satisfy the Gaussian process model is unrealistic in the sense that $c(x,z) > 0$; it may be more appropriate to use a truncated Gaussian or Beta distribution. However, the same techniques apply in practice in the non-Gaussian case; only the mathematics are not as tidy since uncorrelated random variables need not be independent.

Additionally, in practice one must truncate the expansion in (2.16) to include only a finite number of terms. For a second order stationary process (i.e., $K_x(r,s)$ depends only on $\sigma = r-s$) the decay rate of the eigenvalues λ_i as i increases is related to the decay rate of the spectrum $S_x(\nu) = \int K_x(\sigma)e^{-i\nu\sigma}\,\mathrm{d}\sigma$. Alternately, the decay rate of the λ_i is inversely related to the spread of the covariance function, $K_x(r,s) = K_x(\sigma)$. For example, if $X(s,\omega)$ is an uncorrelated (white) process, then $K_x(r,s)$ is an impulse, and the eigenvalues are all equal. In fact, the KL expansion does not converge in this case since the kernel is not in $L^2(0,S)$. On the other hand, if $S_x(\nu)$ has compact support, i.e., $X(s,\omega)$ is band-limited with bandwidth W, then the eigenvalues decay very rapidly, in fact only the eigenvalues up to $i = 2WS+1$ are significant [15]. More detailed estimates are available in [16].

2.3.1 Rational spectrum

The rational spectrum case permits an expansion for which an analytical solution to (2.19) is available. This choice is primarily for convenience and to show that the general techniques apply within the level sets framework. The full derivation is given in [15]. Consider the spectrum for a process $X(s,\omega)$,

$$S_X(\nu)=\frac{2a}{a^2\nu^2+1}. \tag{2.21}$$

The covariance function associated with (2.21) is

$$K_x(r,s)=\exp(-|s-r|/a), \tag{2.22}$$

and a is the correlation length. The correlation length will affect the eigenvalue decay rate, as discussed above. The associated integral equation is

$$\int_0^S \exp(-|s-r|/a)\varphi(r)\mathrm{d}r=\lambda\varphi(s), \quad -S\leq s\leq S. \tag{2.23}$$

The eigenvalue solutions λ_j satisfy

$$\lambda_j=\begin{cases}\frac{2a}{1+a^2\alpha_j^2}, & j \text{ odd},\\ \frac{2a}{1+a^2\beta_j^2}, & j \text{ even}.\end{cases} \tag{2.24}$$

The α_j and β_j are solutions to the following transcendental equations:

$$\begin{cases}1+a\alpha_j\tan(\alpha_j S)=0, & j \text{ odd},\\ a\beta_j+\tan(\beta_j S)=0, & j \text{ even}.\end{cases} \tag{2.25}$$

The associated eigenfunctions are

$$\varphi_j(s)=\begin{cases}\frac{\cos(\alpha_j s)}{\sqrt{S+\sin(2\alpha_j S)/(2\alpha_j)}}, & j \text{ odd},\\ \frac{\sin(\beta_j s)}{\sqrt{S-\sin(2\beta_j S)/(2\beta_j)}}, & j \text{ even}.\end{cases} \tag{2.26}$$

For a process on $[0,2S]$, substitute $r=s+S$ into the above, and (2.23) is still satisfied for $\tilde{\varphi}_j(r)\equiv\varphi_j(r-S)$. The correlation length a controls the eigenvalue decay rate; if a is small, the eigenvalues decay very slowly. For large a, they decay rapidly. For small a, any truncation will result in significant error. Fig. 1 displays the eigenvalues as a function of the number of expansion terms for $a=1,5,10,20$. For $a=1$, the eigenvalues decay quite slowly.

The rational spectrum extends readily to two dimensions as well. Let

$$K_x((r_1,r_2),(s_1,s_2))=\exp(-|s_1-r_1|/a_1-|s_2-r_2|/a_2), \tag{2.27}$$

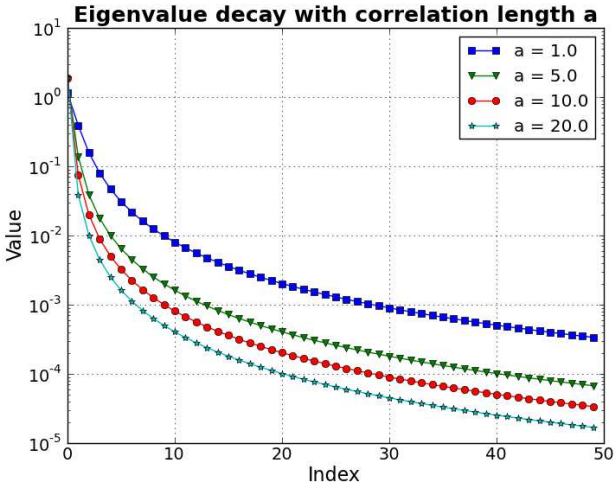

Figure 1: Eigenvalues for the exponential covariance function with correlation length a.

and assume that $\varphi(s_1,s_2)=\varphi^{(1)}(s_1)\varphi^{(2)}(s_2)$. Then the analogue of (2.23) is

$$\begin{aligned}\lambda\varphi^{(1)}(s_1)\varphi^{(2)}(s_2)&=\int\int K_x((r_1,r_2),(s_1,s_2))\,\mathrm{d}r_1\,\mathrm{d}r_2\\&=\int\exp\left(-\frac{|s_1-r_1|}{a_1}\right)\varphi^{(1)}(r_1)\,\mathrm{d}r_1\int\exp\left(-\frac{|s_2-r_2|}{a_2}\right)\varphi^{(2)}(r_2)\,\mathrm{d}r_2\\&=\lambda^{(1)}\varphi^{(1)}(s_1)\lambda^{(2)}\varphi^{(2)}(s_2).\end{aligned}\tag{2.28}$$

So if $a_1\neq a_2$, the eigenvalues and eigenfunctions are just products of the one-dimensional eigenvalues and eigenfunctions. If $a_1=a_2$, each eigenvalue corresponds to two eigenfunctions so the basis functions are

$$\varphi_k(s_1,s_2)=\frac{1}{\sqrt{2}}\left(\varphi_i^{(1)}(s_1)\varphi_j^{(2)}(s_2)+\varphi_j^{(1)}(s_1)\varphi_i^{(2)}(s_2)\right).\tag{2.29}$$

3 Propagating acoustic wavefronts under random sound speed conditions

An acoustic propagation algorithm requires input in the form of a Sound Speed Profile (SSP) specifying $c(x,z)$ which defines the velocity field $\mathbf{V}$, bottom depth as a function of x specifying $z_b(x)$, and a source location to initialize the level set functions. The amplitude equation is neglected in this work in order to study geometric solutions produced by the level set method. Focusing on the SSP, the profiles are often computed using empirical models dependent on measurements of depth, salinity and temperature. Variation in x and y coordinates of physical space is less significant and hence, frequently neglected.

These quantities are typically available as measured data, subject to errors in the equipment used to take the measurements, as well as the unknown variability in the environment. For instance, the SSP varies not only in space, but with time of day. This is especially true in shallow water where warming and cooling patterns in the atmosphere have a predominant effect.

There are also effects of un-modeled (e.g., non-linear) processes on propagation to consider, like internal waves and currents, which are of interest due to the fact, at least for long range propagation, that these un-modeled effects can result in significant deviations of ray paths [17, 18]. It is also common to ignore SSP variability in x (or range in the azimuthal symmetry model), and the effects of many small scatterers on propagation, e.g., bubbles. The method presented here is an application of uncertainty quantification techniques to the level set method as a way to obtain wavefront solutions, in a probabilistic sense, in the presence of uncertainty in the SSP. This capability is valuable since the eigenray problem is highly sensitive to small perturbations in initial conditions. The examples used here are simplified, serving to illustrate that these techniques are applicable to the level set method. It is also worth noting that these techniques are not limited to modeling wave speed uncertainty; the same methods apply to models involving multiple random parameters. Other sources of uncertainty that one might wish to model include, but are not limited to, source and receiver positions and rough surface scattering. The result would be an increase in the dimension of the random space.

3.1 Stochastic collocation

Recall that the goal is to solve (1.6):

$$\frac{\partial \phi_l}{\partial t} = \mathcal{L}\phi_l, \tag{3.1a}$$

$$\mathcal{L} = -\mathbf{V}\cdot\nabla, \tag{3.1b}$$

for $l=1,2$ with $\mathbf{V}$ as in (2.6). Now $\phi_l = \phi_l(t,x,z,\theta;\vec{\xi})$, with $\vec{\xi}=(\xi_1,\cdots,\xi_d)$ a random vector with mutually independent components, $\vec{\xi}:\Omega\to\mathbb{R}^d$. The initial conditions are $\phi_l(0,\cdot)=\phi_l^0(\cdot)$, and appropriate boundary conditions for $(x,z,\theta)\in D\times[-\pi,\pi)$ are available. For example, to initialize a point source at (x_s,z_s), take

$$\phi_1^0(x,z,\theta) = x - x_s, \tag{3.2a}$$

$$\phi_2^0(x,z,\theta) = z - z_s. \tag{3.2b}$$

For a fixed $\omega_0\in\Omega$, ϕ_l is a deterministic function of $(t,x,z,\theta,\vec{\xi}(\omega_0))$, with $\vec{\xi}(\omega_0)$ representing a set of input parameters. Thus one may solve (1.6) using the techniques presented in [4] and [19]. In the stochastic collocation method, one prescribes a set of nodes, $\Theta_M=\{\vec{\xi}^{(k)}\equiv\vec{\xi}(\omega^{(k)})\}_{k=1}^M$ and applies the deterministic solver to compute a corresponding solution set, $\{\phi_l^{(k)}(\cdot;\vec{\xi}^{(k)})\}_{k=1}^M$, $l=1,2$. Formally, the stochastic collocation problem is to

find $\tilde{\phi}_l(\cdot;\vec{\xi})\in\mathbb{P}^d_{N_p}$ such that $\lim_{N_p\to\infty}||\tilde{\phi}_l(\cdot;\vec{\xi})-\phi_l(\cdot;\vec{\xi})||=0$, where the norm is typically the mean square norm. This implies an approximate representation of $\tilde{\phi}_l$ via (2.15). There are two methods for constructing the collocation solution: interpolation and discrete projection (pseudospectral) [14]. In the interpolation approach, one selects the node set Θ_M and constructs the coefficients $\hat{\phi}_{l,n}(t,x,z,\theta)$ by requiring that $\tilde{\phi}_l\left(\cdot;\vec{\xi}^{(k)}\right)=\phi_l^{(k)}\left(\cdot;\vec{\xi}^{(k)}\right)$ at each of the M nodes, $\vec{\xi}^{(k)}$. In discrete projection, one applies quadrature techniques to evaluate the integrals (2.9). Both are valid approaches. This work focuses on the discrete projection approach (3.3), opting for high-dimensional quadrature rather than high-dimensional interpolation. For an example that uses an interpolation approach to stochastic collocation with a parabolic equation (PE) model, see [20]. Both approaches rely on high-dimensional techniques that are still active areas of research.

3.2 Relation to Monte Carlo

Monte Carlo sampling methods are common techniques for solving systems that are dependent on random parameters. The Monte Carlo method uses independent samples drawn randomly from the distribution $F_{\vec{\xi}}(\xi_1,\cdots,\xi_d)$ to generate the $\vec{\xi}^{(k)}$, $k=1,\cdots,M$. That is, one generates the set of nodes Θ_M by sampling from the random distribution, then applies the deterministic solver at each node in the set. The sample mean, $\bar{\phi}_l(t,x,z,\theta)=\frac{1}{M}\sum_{k=1}^M\phi_l^{(k)}(t,x,z,\theta;\vec{\xi}^{(k)})$, and the sample variance, $\sigma^2_{\phi_l}(t,x,z,\theta)=\frac{1}{M-1}\sum_{k=1}^M\left(\phi_l^{(k)}(t,x,z,\theta;\vec{\xi}^{(k)})-\bar{\phi}_l(t,x,z,\theta)\right)^2$, provide estimates for the first and second moments. The advantages of using Monte Carlo are that it is very simple to implement, and that its convergence rate is unaffected by the dimension d of the random space. The disadvantage is that the convergence rate is very slow; the mean-square error decays like $\frac{1}{\sqrt{M}}$. The stochastic collocation method on the other hand, uses a deterministic set of nodes and offers spectral convergence, though convergence slows depending on the smoothness of the underlying solutions and the dimension of the random space.

3.3 Discrete projection

Express $\tilde{\phi}_l$ as the orthogonal gPC projection onto $\mathbb{P}^d_{N_p}$, and drop the subscript l to simplify notation:

$$\tilde{\phi}=\sum_{|\mathbf{n}|=0}^{N_p}\hat{\phi}_{\mathbf{n}}\Psi_{\mathbf{n}}(\vec{\xi}). \tag{3.3}$$

The $\Psi_{\mathbf{n}}(\vec{\xi})$ are the basis functions of the expansion as in (2.13); take them as scaled to form an orthonormal basis. The $\hat{\phi}_{\mathbf{n}}$ are the expansion coefficients,

$$\hat{\phi}_{\mathbf{n}}=\int\phi(\cdot;\xi)\Psi_{\mathbf{n}}(\xi)dF_{\vec{\xi}}(\xi). \tag{3.4}$$

Computing the $\hat{\phi}_{\mathbf{n}}$ yields an expression of the solution $\tilde{\phi}(\cdot;\vec{\xi})$ for any $\vec{\xi}$. This is in contrast to a Monte Carlo procedure, which only provides estimates of moments. Since the function values are only available as discrete samples, quadrature, or if $d>1$, its multivariate extension cubature rule, approximates the integral (3.4). The term *pseudospectral* often describes this technique since the optimal choice of nodes and weights makes this the same as a Galerkin method [21].

The results presented in Section 4 applied Gauss quadrature to compute the integrals (3.4) on a Smolyak [22] grid. For low dimensions, grids formed by taking a tensor product of one-dimensional quadrature grids are adequate, however the number of nodes in a tensor grid grows exponentially with the dimension (i.e., number of uncorrelated random variables in the process expansion). The Smolyak formulation combines lower order tensor products so that the number of function evaluations grows more slowly with dimension d. The Smolyak cubature of level ℓ is [23]

$$\mathcal{Q}_\ell^d f = \sum_{\ell \le |\mathbf{m}| \le \ell+d-1} (-1)^{\ell+d-|\mathbf{m}|-1} \binom{d-1}{|\mathbf{m}|-\ell} \left(\mathcal{Q}^1_{m_1} \otimes \cdots \otimes \mathcal{Q}^1_{m_d}\right) f, \tag{3.5}$$

where $\mathbf{m}=(m_1,\cdots,m_d)$ is a multi-index and $\mathcal{Q}^1_q$ represents a one-dimensional quadrature using q nodes. The effect is to use only a subset of the nodes in the full d-dimensional tensor grid. Fig. 2 compares a full tensor grid on $[-1,1]\times[-1,1]$ with a Smolyak sparse grid. For further background on sparse quadrature, we refer the reader to [22–24] and the references therein.

The Gaussian nature of the examples studied in this work requires cubature on unbounded intervals. One approach to this problem is to truncate the domain. Another is to use a mapping to a bounded domain and use, for example, Legendre points. Domain truncation is not unreasonable for problems involving Gaussian PDFs due to the exponential decay, though Gauss-Hermite quadrature appeared to offer improved performance in our experiments. This work does not address domain mapping, but [25] offers a recent review of the different approaches.

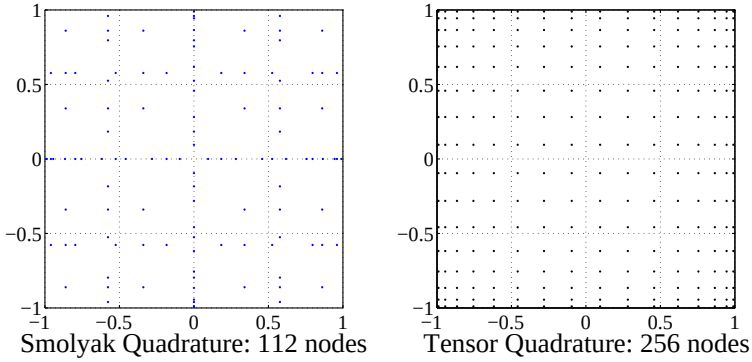

Figure 2: Example of Smolyak sparse grid (left) and full tensor grid (right) in two dimensions.

3.4 Computing the statistics

The stochastic collocation yields an approximate solution $\tilde{\phi}(\cdot;\vec{\xi})$ for any $\vec{\xi}$ in the random space. The moments are then readily computed by passing the expectation over the sum (3.3) and applying the orthogonality condition, e.g.,

$$\mathbb{E}[\tilde{\phi}] = \hat{\phi}_0, \tag{3.6}$$

$$\mathrm{Var}[\tilde{\phi}] = \sum_{|\mathbf{n}|=1}^{N_p} \hat{\phi}_{\mathbf{n}}^2. \tag{3.7}$$

Thus, convenient expressions are available for the study of errors and sensitivity analysis. These expressions provide a means for verification of the method when analytical solutions are available for the level set functions, which may not have physical significance away from the zero level sets. To extract physical meaning from these quantities, one must consider moments of functions (or functionals) of the level set functions themselves. For example, one might study the wavefront normals derived from the gradients, or extract information about the pressure amplitude which is related to the wavefront curvature and can be tracked simultaneously using level-sets-based techniques similar to those presented in [26–28]. The extraction of physically meaningful, statistical information from the level set functions has not been fully studied (to the author's knowledge). Closely related work by Azaïs, León, and Wschebor [29, 30] on the application of Rice formulae to study specular points and zero crossings might serve as a starting point in this direction.

4 Results

4.1 Single uniform random variable

The first experiment performs a basic study using a single random parameter. For this, let

$$c(x,z) = c_0 + \epsilon\xi, \tag{4.1}$$

where $\epsilon = 0.3$ and ξ is a uniform random variable on $[-1,1]$ so that $\mathbb{E}[\xi] = 0$ and $\mathrm{Var}[\xi] = \frac{1}{3}$. This suggests that a Legendre polynomial chaos expansion is appropriate, and the samples $\left\{\xi^{(k)}\right\}_{k=0}^{N_p}$ are given by the Gauss-Legendre quadrature points. The model corresponds to a case in which it is known that the sound speed is constant, but there is uncertainty about what that speed is. This case allows for the computation of errors since the solution is known given initial conditions for a point source,

$$\phi_1(t,x,z,\theta;\xi) = x - (c_0 + \epsilon\xi)t\cos\theta, \tag{4.2}$$

$$\phi_2(t,x,z,\theta;\xi) = z - z_s - (c_0 + \epsilon\xi)t\sin\theta. \tag{4.3}$$

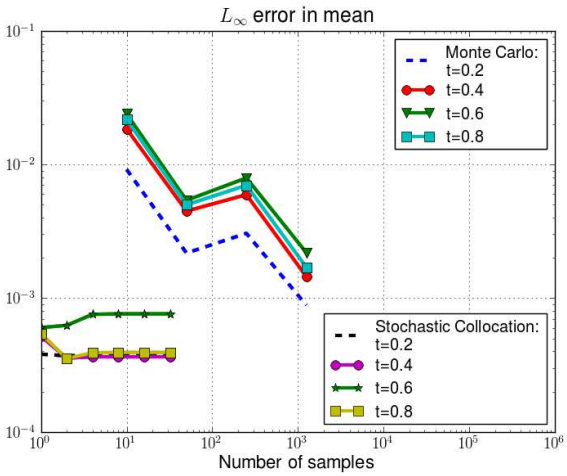

Figure 3: Convergence of level set functions in mean as a function of the number of function evaluations, computed at four separate times. Sound speed is a uniform random variable.

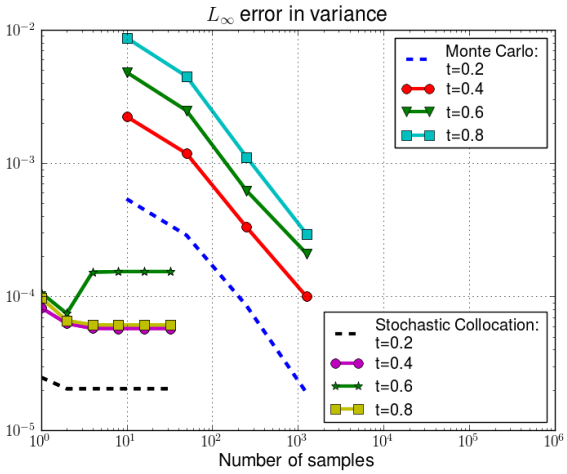

Figure 4: Convergence of level set functions in variance as a function of the number of function evaluations, computed at four separate times. Sound speed is a uniform random variable.

The wavefront solutions correspond to circles of radius $(c_0+\epsilon\xi_i)t$ for each random sample ξ_i, at time t. A Monte Carlo sampling scheme applied to the same problem provides a comparison. Figs. 3 and 4 show the errors in computed mean and variance of $\mathbf{\Phi}$ respectively, computed using the L_∞ norm for both the Monte Carlo and Stochastic Collocation approaches at four fixed times. Since the gPC expansion is exact for the single uniform random variable model, the stochastic collocation converges immediately, with the error attributable to numerical quadrature and the error in the level set method solver only. The Monte Carlo simulation requires about 1000 samples to converge to the same

level. It is also noteworthy that the errors are time-dependent; this is a known result of the application of gPC expansions to hyperbolic problems [14]. As the time at which the errors are computed increases, so does the number of samples required for Monte Carlo to match the errors in the stochastic collocation. For this simple case, the stochastic collocation method has a distinct advantage.

4.2 Gaussian random field

Now let

$$c(x,z) = c_0 + X(x,z;\omega), \tag{4.4}$$

where $X(x,z;\omega)$ is a zero-mean, Gaussian random field with exponential covariance as in (2.27). A KL expansion decomposes the process into independent, Gaussian random variables. The techniques in this section then apply directly to the expansion. The correlation lengths applied here are $a_x = 5.0$ and $a_z = 100.0$. These values are large to ensure the eigenvalues decay rapidly so as to limit the amount of computation. The number of modes was limited by feasible computational time, yet the stochastic collocation result appears to have converged (although only two terms are retained in the KL expansion), whereas the Monte Carlo result does not, even with an order of magnitude more function evaluations. An optimization of the level sets code would be necessary to permit larger expansions. For this example, eigenvalues less than 10^{-1} were neglected. Figs. 5 and 6 show how the results vary for fixed dimension $d = 2$ (d corresponds to the number of modes retained in the KL expansion) with the number of evaluations of the level set method for the same scenario. The errors are clearly smaller for the collocation approach at a comparable number of function calls. The result from Monte Carlo with $N_s = 50{,}000$ serves as the point of comparison in the absence of exact solutions.

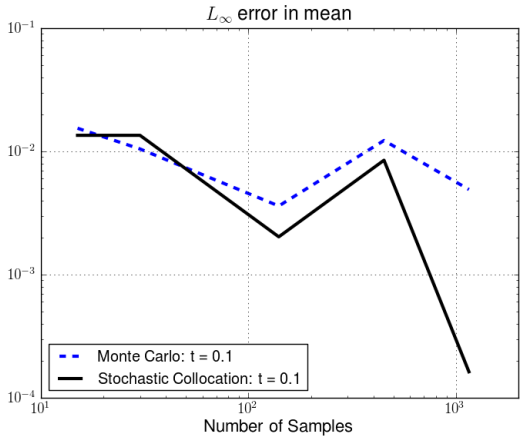

Figure 5: Convergence in mean for sound speed represented by a Gaussian process with constant mean versus number of function evaluations, evaluated at time $t = 0.1$ seconds

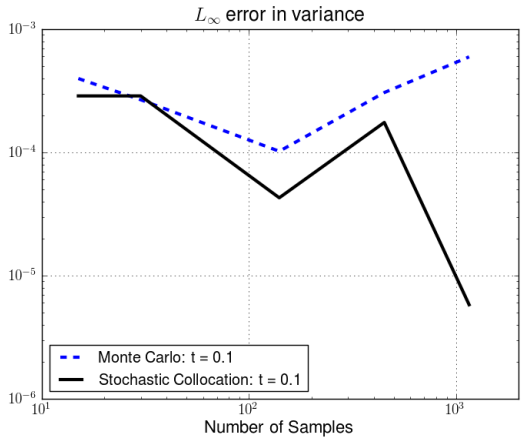

Figure 6: Convergence in variance for sound speed represented by a Gaussian process with constant mean versus number of function evaluations, evaluated at time $t=0.1$ seconds

The goal of this work is to apply stochastic collocation to the level set functions for geometric acoustic wavefront tracing not only for analysis purposes, but also to simulate the propagation of acoustic wavefronts in a medium with uncertain sound speed. The final two examples in this section demonstrate this application. One first computes and the gPC expansion coefficients, $\hat{\phi}_{l,n}(t,x,z,\theta)$, $l=1,2$, for the level set functions via stochastic collocation over the desired spatial and temporal domains. Then, an online simulation procedure would only need to supply realizations of the expansion random variables to compute an instance of a wavefront. Fig. 7 shows realizations of the extracted wavefronts from the computed coefficients of the level set function components provided by a stochastic collocation formulation with $d=2$ and $N_p=4$, for the above sound speed process, i.e., constant with additive zero-mean Gaussian process.

The last example uses data processed at Woods Hole Oceanographic Institute (WHOI) as part of the Shallow Water 2006 (SW06) experiment [8,31]. The data were preprocessed and contain values at 15 depths over time; there is no range (or x) dependence and the time variability is small. A cubic spline fit provides a smooth representation of the data, providing estimates of $\frac{\partial c}{\partial z}$. One time sample of the spline-fitted profile data is shown in Fig. 8. This is a typical shallow water profile — the region of higher sound speed near the surface (first ten meters) is a result of higher temperatures caused by, for example, heating due to daylight. Below this region, the temperatures cool. Thus the sound speed decreases, and becomes more stable with depth, appearing approximately constant at the last ten meters. In deeper water, one would typically see a gradual cooling due to the increased pressure. The effect this has on the propagation is to create faster spreading of the wavefronts near the surface as opposed to near the sea bottom.

Fig. 9 shows realizations of the extracted wavefronts from the computed coefficients of the level set function components provided by a stochastic collocation formulation with $d=3$ and $N_p=3$ using the sound speed profile $c_0(z)$ in Fig. 8 with an additive

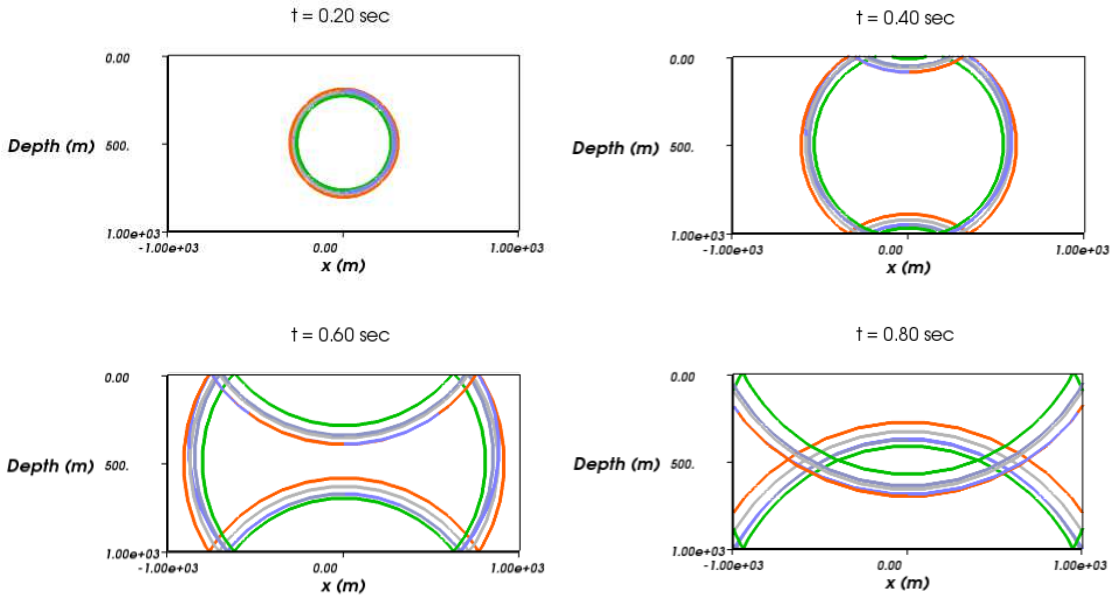

Figure 7: Time snapshots of wavefronts generated from random samples of level set functions for data with a constant sound speed added to a Gaussian random process.

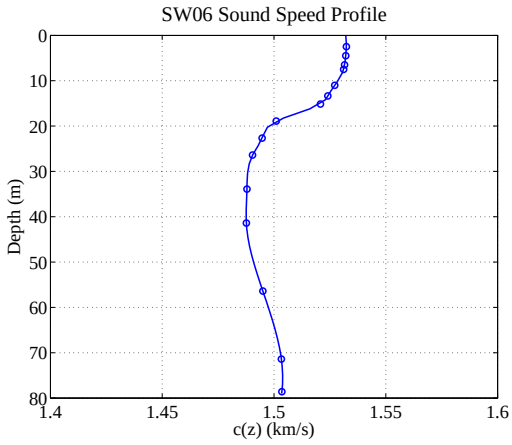

Figure 8: Sound speed data versus water column depth from SW06 experiment.

Gaussian process. The subfigures show the wavefronts at different times. The results are consistent with the mean sound speed profile shown in Fig. 8, with the wavefronts spreading faster near the surface, and slower toward the bottom. However, each realization has slightly different displacements at as a result of the random perturbations in the sound speed.

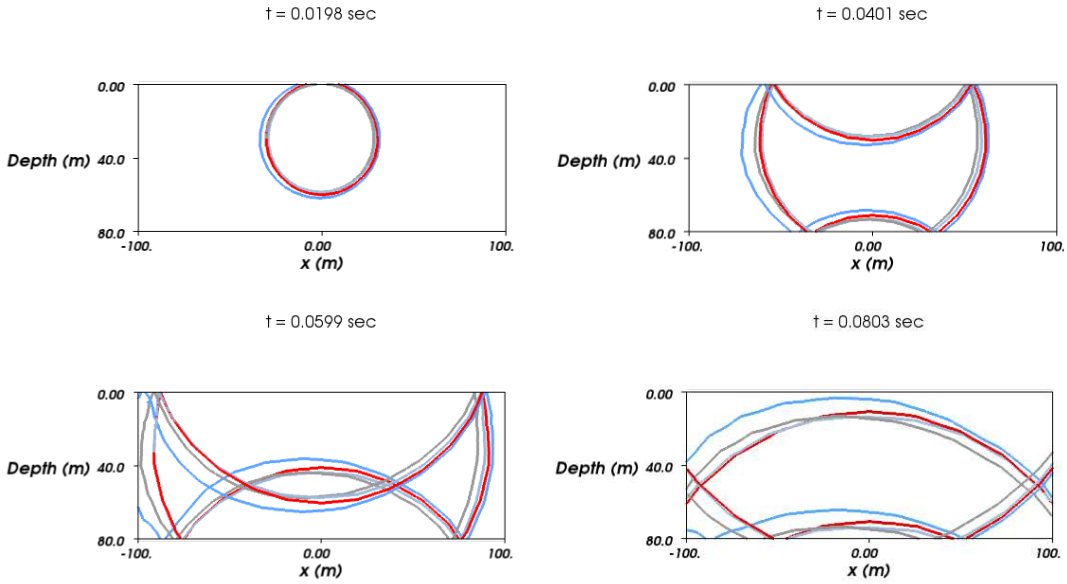

Figure 9: Time snapshots of wavefronts generated from random samples of level set functions for the SW06 SSP data with a Gaussian random process.

5 Conclusion

This work explored the application of stochastic collocation to a level set method in order to simulate wavefronts propagating in uncertain environments. The particular approach taken permits a functional representation of the wavefront solution in terms of independent random variables. Thus in a simulation program, one could precompute the collocation coefficients in order to generate realizations of wavefronts propagating in the presence of uncertainty. The stochastic collocation solutions also, under certain conditions, converge to the true moments much faster than traditional Monte Carlo approaches. The results are very promising, as the technique is general enough to apply readily to represent other random parameters. The complications of high dimensional representations in random space do suggest that further work is needed. First, the implementation of the level set method should be optimized so that it is more feasible to run the large number of simulations required for larger expansions. It would also be reasonable to look at representing band-limited processes using prolate spheroidal wave functions as a gPC basis as described in [15,16]. These factors are important to consider, particularly if one wishes to permit uncertainty from other sources such as boundary locations.

Acknowledgments

The author would like to thank Dr. Drumheller and Dr. Soukup of ONR for their support of this program. I also thank Art Newhall and others in the Applied Ocean Physics

& Engineering Department at WHOI for access to the pre-processed SSP data from the SW06 experiment. This work is also partially funded by the Science, Mathematics, And Research for Transformation (SMART) program. Additionally, I wish to thank Dr. Jan Hesthaven of Brown University for his technical oversight and advice.

References

[1] F. Jensen, W. Kuperman, M. Porter, and H. Schmidt, Computational Ocean Acoustics. Modern Acoustics and Signal Processing, New York: Springer, second ed., 2011.
[2] P. Roux, B. Cornuelle, W. Kuperman, and W. Hodgkiss, The structure of raylike arrivals in a shallow-water waveguide, J. Acoust. Soc. Amer., vol. 124, pp. 3430–39, 2008.
[3] A. Singer, J. Nelson, and S. Kozat, Signal processing for underwater acoustic communications, Communications Magazine, IEEE, vol. 47, pp. 90 –96, January 2009.
[4] S. Martinelli, An application of the level set method to underwater acoustic propagation, Commun. Comput. Phys., vol. 12, no. 5, pp. 1359–1391, 2012.
[5] S. Osher and J. Sethian, Fronts propagating with curvature dependent speed: Algorithms based on Hamilton-Jacobi formulations, J. Comput. Phys., vol. 79, pp. 12–49, 1988.
[6] S. Osher, L.-T. Cheng, M. Kang, H. Shim, and Y.-H. Tsai, Geometric optics in a phase-space-based level set and Eulerian framework, J. Comput. Phys., vol. 179, pp. 622–648, 2002.
[7] O. Godin, Restless rays, steady wave fronts, J. Acoust. Soc. Amer., vol. 122, pp. 3353–3363, 2007.
[8] S. Martinelli, A Level-Sets-Based Wavefront Propagation Method for Underwater Acoustics. PhD thesis, Brown University, May 2012.
[9] D. Xiu and J. Hesthaven, High-order collocation methods for differential equations with random inputs, SIAM J. Sci. Comput., vol. 27, pp. 1118–1139, 2005.
[10] C. Chauviere, J. Hesthaven, and L. Lurati, Computational modeling of uncertainty in time-domain electromagnetics, SIAM J. Sci. Comput., vol. 28, pp. 751–775, 2006.
[11] F. Nobile, R. Tempone, and C. Webster, A sparse grid stochastic collocation method for partial differential equations with random input data, SIAM J. Numer. Anal., vol. 46, pp. 2309–2345, 2008.
[12] J. Preston, T. Tasdizen, C. Terry, A. Cheung, and R. Kirby, Using the stochastic collocation method for the uncertainty quantification of drug concentration due to depot shape variability, IEEE Trans. Biomed. Eng., vol. 56, no. 3, pp. 609–620, 2009.
[13] T. Pätz and T. Preusser, Segmentation of stochastic images using level set propagation with uncertain speed, J. Math. Imaging Vis., pp. 1–21, 2013.
[14] D. Xiu, Numerical Methods for Stochastic Computations: A Spectral Method Approach. Princeton, New Jersey: Princeton University Press, 2010.
[15] H. Van Trees, Detection, Estimation, and Modulation Theory: Part I. New York: Wiley-Interscience, paperback ed., 2001.
[16] H. Widom, Asymptotic behavior of the eigenvalues of certain integral equations II, Arch. Ration. Mech. An., vol. 17, pp. 215–229, 1964.
[17] T. Duda, Ocean sound channel ray path perturbations from internal-wave shear and strain, J. Acoust. Soc. Amer., vol. 118, pp. 2899–2903, 2005.
[18] J. Colosi, Geometric sound propagation through an inhomogeneous and moving ocean: Scattering by small scale internal wave currents, J. Acoust. Soc. Amer., vol. 119, pp. 705–708, 2006.

[19] S. Martinelli, Numerical boundary conditions for specular reflection in a level-sets-based wavefront propagation method, Commun. Comput. Phys., vol. 14, no. 2, pp. 509–536, 2013.
[20] S. Finette, A stochastic response surface formulation of acoustic propagation through an uncertain ocean waveguide environment, J. Acoust. Soc. Amer., vol. 126, pp. 2242–2247, 2009.
[21] J. Boyd, Chebyshev and Fourier Spectral Methods. New York: Dover, second ed., 2001.
[22] S. Smolyak, Quadrature and interpolation formulas for tensor products of certain classes of functions, Soviet Math. Dokl., vol. 4, pp. 240–243, 1963.
[23] T. Gerstner and M. Griebel, Numerical integration using sparse grids, Numerical Algorithms, vol. 18, pp. 209–232, 1998.
[24] E. Novak and K. Ritter, Simple cubature formulas with high polynomial exactness, Constr. Approx., vol. 15, pp. 499–522, 1999.
[25] J. Shen and L.-L. Wang, Some recent advances on spectral methods for unbounded domains, Commun. Comput. Phys., vol. 5, pp. 195–241, 2009.
[26] S. Jin, H. Liu, S. Osher, and Y.-H. Tsai, Computing multivalued physical observables for the semiclassical limit of the Schrödinger equation, J. Comput. Phys., vol. 205, pp. 222–241, 2005.
[27] S. Jin, H. Liu, S. Osher, and R. Tsai, Computing multi-valued physical observables for the high frequency limit of symmetric hyperbolic systems, J. Comput. Phys., vol. 210, pp. 497–518, 2005.
[28] H. Liu, S. Osher, and R. Tsai, Multi-valued solution and level set methods in computational high frequency wave propagation, Communications in Computational Physics, vol. 1, no. 5, pp. 765–804, 2006.
[29] J.-M. Azaïs, J. León, and M. Wschebor, Some applications of Rice formulas to waves, ArXiv e-prints, Oct. 2009, 0910.0763v1.
[30] J.-M. Azaïs, J. León, and M. Wschebor, Rice formulae and Gaussian waves, Bernoulli, vol. 17, no. 1, pp. 170–193, 2011.
[31] A. Newhall, T. Duda, et al., Acoustic and oceanographic observations and configuration information for the WHOI moorings from the SW06 experiment, Tech. Rept. WHOI-2007-04, Woods Hole Oceanographic Institute, May 2007.